Scientific Research Publishing

Computational Chemistry, 2022, 10, 121-137
https://www.scirp.org/journal/cc
ISSN Online: 2332-5984
ISSN Print: 2332-5968

A Statistical Evaluation of Uncoupling Protein 1 in the Limited Area of Brown Adipose Tissue by Immunoelectron Microscopy

Xiaomin Dong[1], Seiichi Chiba[1*], Tatsuo Shimada[2], Fumihiko Hamada[1]

[1]Department of Anatomy, Faculty of Medicine, Oita University, Oita, Japan
[2]Emeritus Professor, Faculty of Medicine, Oita University, Oita, Japan
Email: *schiba@oita-u.ac.jp

How to cite this paper: Dong, X.M., Chiba, S., Shimada, T. and Hamada, F. (2022) A Statistical Evaluation of Uncoupling Protein 1 in the Limited Area of Brown Adipose Tissue by Immunoelectron Microscopy. *Computational Chemistry*, **10**, 121-137.
https://doi.org/10.4236/cc.2022.103006

Received: July 1, 2022
Accepted: July 22, 2022
Published: July 29, 2022

Abstract

Uncoupling protein 1 (UCP1) expressed by the brown adipose tissue (BAT) in the mitochondrial crista acts as a homeostatic thermogenerator of eutherians. The evaluation of UCP1 expression in the BAT offers significant scientific insight, especially in studies targeting limited areas such as the periarterial and pericardial regions of small experimental mammals. However, the negligible amount of this adipose tissue would render the general quantitative evaluation of the protein unreliable because of lipid contamination and low protein concentration. To address this problem, we quantitatively evaluated UCP1 expression in the mitochondrion of the mouse interscapular BAT using immunoelectron microscopy and immunohistochemical studies using a combination of primary and secondary antibodies in scheme A (rabbit anti-UCP1 IgG/gold particle-conjugated goat anti-rabbit IgG), B (rabbit IgG/gold particle-conjugated goat anti-rabbit IgG), C (rabbit anti-UCP1 IgG/gold particle-unconjugated goat anti-rabbit IgG), and D (rabbit IgG/gold particle-unconjugated goat anti-rabbit IgG). Scheme A shows the immunopositive reaction of obvious gold particles in the mitochondrial area, whereas other procedures revealed less distinctive reactions. The distinctive gold particle immunoreaction comprised electrical high-density spots with a mean diameter of >5 nm. However, in scheme B, the electrical high-density spots were scattered outside the mitochondrion and were significantly smaller than 4 nm; schemes C and D demonstrated few immunoreactions. Logistic regression analysis between schemes A and B showed that the threshold diameter of the electrical high-density spots measuring >5 nm indicated a true positive immunoreaction to anti-UCP1 antibody specifically in the mitochondrial area. Minor statistical difference was observed in the primary anti-UCP1 antibody between polyclonal IgG and monoclonal antibodies. Therefore, im-

munoelectron microscopy might be useful for evaluating negligible protein expression in some limited areas, such as UCP1 expression in the BAT of small experimental animals.

Keywords

Uncoupling Protein 1 (UCP1), Brown Adipose, Immunoelectron Microscopy, Immunohistochemical Staining, Logistic Regression Analysis

1. Introduction

Uncoupling protein 1 (UCP1) is a thermogenic biomolecule expressed in the mitochondrial crista of adipocytes in the brown adipose tissue (BAT) of mammals [1] [2] [3] [4]. The biological functions of UCP1 include thermogenesis and antioxidative reactions that enable the conversion of free electrons for heat generation. Therefore, evaluation of the expression of UCP1 in the BAT may give an insight into energy homeostasis involving glucose and lipid metabolism, as well as oxidative reactions [5]. The involvement of periarterial and pericardial BAT in metabolic and arteriosclerotic disorders emphasizes the need to evaluate UCP1 function around the arteries and heart [6] [7] [8] [9]. Nevertheless, some difficulties exist in the quantitative evaluation of UCP1 expression in lipid-rich organs such as BAT around relatively restricted areas, such as the periarterial and pericardial regions of small experimental animals such as mice [10] [11]. A successful approach to this problem was shown by Cinti *et al*. using an immunoelectron microscope [12], and developed by other researchers using gold particles conjugated to secondary antibodies [13] [14] [15] [16] [17]; however, the numerical characteristics of the immunopositive reactions remain obscure.

In this study, we quantitatively evaluated the expression of UCP1 in the interscapular BAT of mice by immunohistochemical staining using a gold particle-conjugated secondary antibody and electron microscopy. In addition, we statistically compared the diameters and densities of high-intensity electron signals of gold particles in the mitochondrial area under staining conditions with or without primary or secondary antibodies.

2. Material and Methods

2.1. Animals

Eight male C57Bl/6 mice aged approximately 10 weeks with an initial weight of approximately 22 - 24 g were used in this study. Four mice were housed per cage in a soundproof room under a 12 h/12 h light/dark cycle (lights on at 07:00 h) and fed a standard laboratory diet and tap water *ad libitum*. All procedures were conducted according to the Oita University Guide for the Care and Use of Laboratory Animals, based on the National Institutes of Health guidelines, and approved by the Animal Care Committee of Oita University (No. 200101).

2.2. Chemicals

Rabbit polyclonal antibodies against UCP1 (ab10983, Abcam Inc., Cambridge, UK) and rabbit monoclonal antibody against UCP1 (EPR20381, Abcam Inc., Cambridge, UK) were used as primary antibodies for immunohistochemical staining. Rabbit polyclonal IgG (ab37415, Abcam Inc., Cambridge, UK) and rabbit monoclonal IgG (EPR25A, Abcam Inc., Cambridge, UK) were used as primary IgG isotype controls to identify false positives in the electron microscopic immunohistochemical staining method. These primary antibodies were labeled by a gold-conjugated (5.4 nm mean diameter) goat anti-rabbit IgG antibody (GAR-70802/1, Aurion, Wageningen, NLD) as the secondary antibody in the immunoelectron microscopic analysis. Goat anti-rabbit IgG (G0388, TCI, Tokyo, JP) was used as an isotype control for the secondary antibody.

2.3. Apparatus and Software

Transmission electron microscopy and immunoelectron microscopy were performed using a model H-7650 microscope (Hitachi, Tokyo, Japan). ImageJ (U.S. National Institutes of Health, Bethesda, Maryland, USA, https://imagej.nih.gov/ij/, 1997-2017) was used for image analysis, and SAS (JMP Pro 14, SAS Institute, Cary, NC, US) was used for statistical analyses.

2.4. Experimental Procedures

2.4.1. Sample Collection

All animals were anesthetized at 10:00 h with pentobarbital sodium (150 mg/kg intraperitoneal [i.p.]) and perfused through the left ventricle with ice-cold saline followed by either 4% paraformaldehyde in 0.05 M cacodylate buffer (pH 7.4) for light microscopy, fluorescence microscopy, and immunoelectron microscopy or 50% Karnovsky's fixative solution [18] for transmission electron microscopy. The hearts and aortae were excised and fixed overnight.

2.4.2. Four Schemes of Immunoelectron Histochemical Staining Regimes

To confirm the accurate immunoelectron reaction with UCP1 in the BAT, we tested four schemes of immunoelectron histochemical staining. Scheme (A) served as a regular protocol using the primary antibody to UCP1 and the gold-conjugated secondary antibody. The second scheme (B) served as a protocol missing the specific primary antibody, combined with a nonspecific immunoglobulin as a primary antibody and a gold-conjugated secondary antibody. The third scheme (C) served as a protocol missing highlight by the gold standard, combining the primary antibody to UCP1 and a nonspecific immunoglobulin as a secondary antibody. The fourth scheme (D) served as a control protocol, combining a nonspecific immunoglobulin as the primary antibody and a nonspecific immunoglobulin as the secondary antibody. During the treatment with the primary antibody, rabbit polyclonal anti-UCP1 immunoglobulin (IgG) or rabbit monoclonal anti-UCP1 IgG was used. Gold-conjugated goat anti-rabbit IgG was used as the secondary antibody. For nonspecific rabbit IgG and goat

IgG, rabbit polyclonal IgG, rabbit monoclonal IgG, and goat IgG were used.

2.4.3. Immunoelectron Microscopy

The collected samples were cut into very fine pieces, fixed in 4% paraformaldehyde in 0.05 M cacodylate buffer (pH 7.4) for 2 h at 4˚C, and rinsed with 0.1 M cacodylate buffer (pH 7.4). The specimens were dehydrated in an ascending ethanol wash series and embedded in LR White resin (London Resin Co. Ltd., London, UK). Ultrathin sections were cut using an ultramicrotome and mounted onto copper grids. The samples were rinsed thrice with phosphate-buffered saline (PBS) for 3 min, incubated in 1% bovine serum albumin (BSA) in PBS (BSA-PBS; 0.01 M phosphate buffer + 0.15 M sodium chloride [NaCl], pH 7.2) for 30 min at room temperature, and then incubated with rabbit polyclonal (or monoclonal) IgG anti-UCP1 primary antibody (1/10,000) overnight at 4˚C. This was followed by rinsing in BSA-PBS for 30 min at room temperature and incubation with gold-conjugated goat anti-rabbit IgG antibody (1/40) for 1 h at room temperature. Samples were then rinsed thrice with PB (0.01 M, pH 7.4) for 30 min at room temperature, followed by rinsing with distilled water for 10 s. Next, the samples were subjected to the physical development treatment as mentioned above. Briefly, the samples were incubated in a mixture of solutions A and B for 28 min at 23˚C and then rinsed four times in distilled water for 5 min. Finally, the samples were dried and stained with distilled water containing 1% methanolic uranyl acetate and 0.08% lead citrate, in the same manner as for transmission electron microscopy (TEM) [19]. The same protocol was also applied in schemes (C and D) using nonspecific IgG as primary or secondary antibodies.

2.5. Digital Image Analysis of the Outcome of Immunoelectron Microscopy

The samples used for immunoelectron microscopic analysis were divided into the following four groups: For schemes A and B, polyclonal rabbit IgG as the "primary" anti-UCP1 antibody and gold-conjugated polyclonal goat IgG as the "secondary" anti-rabbit antibody (polyclonal UCP1+/G+), polyclonal IgG for the anti-UCP1 antibody(−) with gold-conjugated polyclonal goat IgG for the anti-rabbit antibody (polyclonal UCP1−/G+). For schemes A and B, monoclonal rabbit IgG for the anti-UCP1 antibody(+) with gold-conjugated polyclonal goat IgG for the anti-rabbit antibody (monoclonal UCP1+/G+), and monoclonal IgG for the anti-UCP1 antibody(−) with gold-conjugated polyclonal goat IgG for the anti-rabbit antibody (monoclonal UCP1−/G+). Negative controls for immunoelectron microscopic analysis were prepared for four additional groups. Schemes C and D in polyclonal IgG treatment, polyclonal rabbit IgG for the anti-UCP1 antibody with polyclonal goat IgG for the anti-rabbit antibody (polyclonal UCP1+/G−), polyclonal rabbit IgG with polyclonal goat IgG for the anti-rabbit antibody (polyclonal UCP1−/G−). Schemes C and D in monoclonal IgG treatment, monoclonal rabbit IgG for the anti-UCP1 antibody with monoclonal goat

IgG for the anti-rabbit antibody (polyclonal UCP1+/G−), monoclonal rabbit IgG with the monoclonal goat IgG for the anti-rabbit antibody (polyclonal UCP1−/G−). All the samples mounted on copper grids were observed using electron microscopy. Immunoelectron microscopic reactivity was recorded using 30 images with a magnitude of 1/100,000 for each sample. Each image was evaluated for the following three values: 1) mitochondrial area, 2) diameter of the intensive immunoreactive dots, and 3) count of the intensive immunoreactive dots in the mitochondrial area. The diameter of each intensive immunoreactive dot provided information analogous to a 6 nm diameter gold corpuscle in the secondary antibody. The mitochondrial area and count of the intensive immunoreactive dots around or above 6 nm in diameter identified the density of immunoreactivity to UCP1 in the mitochondrial area of the BAT.

2.6. The Reliability of Immunoreactivity of Primary Anti-UCP1 Antibodies with Gold-Conjugated Secondary Antibody in Mitochondrial Areas

To estimate the sensitivity and specificity of immunoelectron staining using primary anti-UCP1 polyclonal or monoclonal IgG antibodies, the numerical data of the diameters of the immunoreactive dots were obtained by a logistic regression analysis. This analysis estimated the reliability between the independent variable of the presence or absence of the UCP1 antibody and the dependent variable of the diameter of the immunoreactive dots in the mitochondrial areas.

2.7. Statistical Analysis

The results were expressed as mean values with associated standard errors. Normality was confirmed using the Shapiro-Wilk test, and continuous variables were compared using analysis of variance (ANOVA). The contribution of independent variables to the properties of dependent variables and the evaluation of suitability between several models were confirmed by a multivariate multinomial logistic regression analysis. The area under the curve (AUC), sensitivity, specificity, and cutoff values were also calculated using integrated logistic models. Statistical significance was set at $P < 0.05$. All statistical analyses were conducted using the SAS software (JMP Pro 14, SAS Institute, Cary, NC, US).

3. Results

3.1. Morphology of the BAT

In comparison with the white adipose tissue (WAT), the BAT exhibited a multilocular appearance upon staining with hematoxylin and eosin (Supplementary **Figure S1**). Ultrastructure evaluation revealed the abundance of mitochondria with well-developed cristae in the cytoplasm as one of the distinctive features of BAC (Supplementary **Figure S2**). Immunohistochemical staining of UCP1 using a polyclonal IgG antibody against UCP1 (polyclonal UCP1 antibody) revealed positive reactions with visible brown staining in the cytoplasm of the BAT (Sup-

plementary Figure S3). Similarly, immunohistochemical staining with polyclonal UCP1 antibody exhibited prominent positive reactions in black (Supplementary Figure S4) or red fluorescence (Supplementary Figure S5). The precise site of UCP1 expression in the cytoplasm was observed by immunoelectron staining using TEM. Positive immunoreaction of polyclonal UCP1 antibody conjugated with gold particles with a mean diameter of 5.4 nm was identified on the inner membrane of the mitochondrial crista of the BAC as compared to that in the WAT and negative controls (Supplementary Figure S6).

3.2. Immunoelectron Staining of BAT

All numerical values were normally distributed according to the Shapiro–Wilk test. We detected two patterns in the immunoelectron reaction, represented by clusters of gold particles. The first pattern was the density of clustered gold particles appearing as immunoelectron-positive reactions in the mitochondrial area. Polyclonal and monoclonal UCP1+/G+ (scheme A) exhibited similar immunoelectron-positive reactions in the inner membrane of the mitochondrial crista of BAC compared to the negative controls (Figure 1 and Figure 2). The outcomes of the immunoelectrical staining in UCP1+/G− (scheme C) and UCP1−/G− (scheme D) showed no signals of immunoreaction, in which there was no difference between UCP1+/G− or UCP1−/G− and plane electron microscope image, then the images of UCP1+/G− and UCP1−/G− were not demonstrated. Quantitative analyses revealed a significant increase in the density of immunoelectron-positive reactions to polyclonal UCP1+/G+ (scheme A), as well as to monoclonal UCP1+/G+ (scheme A), compared with UCP1−/G+ (scheme B) (Figure 3). No significant differences were found between polyclonal and monoclonal UCP1+/G+ (Figure 3). Computerized measurement of the diameter of the clustered gold particles indicated a significant increase in the diameter of polyclonal and monoclonal UCP1+/G+ compared to UCP1−/G+ (Figure 4). Remarkably, no significant differences were found between polyclonal and monoclonal UCP1+/G+ (Figure 4). The cutoff values in the logistic regression analysis of the diameter of the clustered gold particles were 5.647 nm (sensitivity, 96.480%; specificity, 96.48%; AUC = 0.997, $P < 0.001$) when using the polyclonal UCP1 antibody and 5.140 nm (sensitivity 98.810%, specificity 97.34%, and AUC = 0.999, $P < 0.001$) when using the monoclonal UCP1 antibody (Figure 5).

Overall, the positive reaction of clustered gold particles was more impressive when the monoclonal UCP1 antibody was used, whereas little quantitative significance was found in the density and diameter between the polyclonal and monoclonal UCP1 antibodies.

4. Discussion and Conclusions

The BAT exhibited a multilocular appearance with small fat droplets and abundant mitochondria along with UCP 1 expression in the cytoplasm (Supplementary Figures S1-S6). The expression site of UCP1 was confirmed in the inner

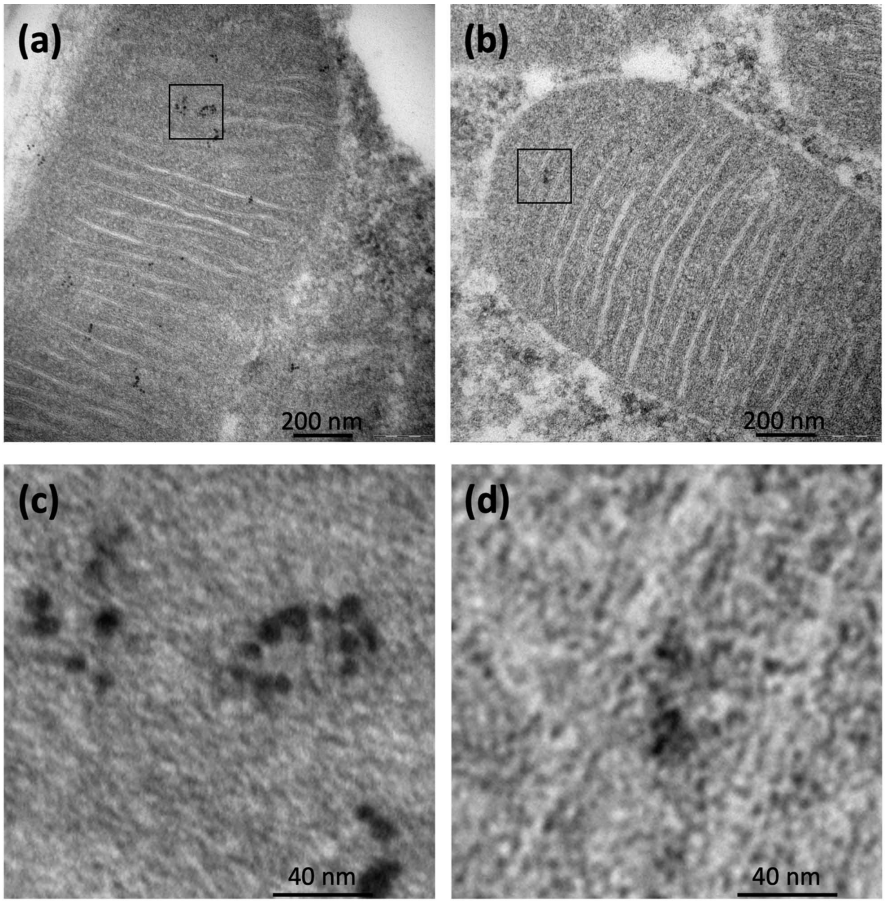

Figure 1. Visualized patterns of gold particles following polyclonal rabbit IgG treatment of the brown adipose tissue (BAT). Region of interest was focused on the mitochondrial area. (a) UCP1+/G+, scheme A in polyclonal IgG with polyclonal rabbit anti-UCP1 IgG and gold particle-conjugated goat anti-rabbit IgG. Solid aggregation of gold particles was observed in the mitochondrial area. Open square was the domain of the magnification exhibited in c (c). Solid bar represents 200 nm, ×50,000 magnification. (b) UCP1−/G+, scheme B in polyclonal IgG with polyclonal rabbit IgG and gold particle-conjugated goat anti-rabbit IgG. Faint spots of gold particles were observed in the mitochondrial area. Open square was the domain of the magnification exhibited in below. Solid bar represents 200 nm, ×50,000 magnification. (c) Magnified image of the square in a. The aggregation of massive signals of gold particles was confirmed. Solid bar represents 40 nm, ×200,000 magnification. (d) Magnified image of the square in b. The weak signals of gold particles were observed. Solid bar represents 40 nm, ×200,000 magnification.

membrane of the mitochondrial crista by immunohistochemical staining and electron microscopy (**Figure 1** and **Figure 2** and Supplementary **Figure S6(b)**). Immunoelectron images of UCP1 revealed the immunoreactive clusters of gold particles immunochemically conjugated to the UCP1 antibody. Next, gold particles were significantly identified using the diameter indicated by the manufacturer in the univariate logistic regression analysis (**Figure 5**). A quantitative comparison of the patterns of the immunoreactive clusters between the polyclonal IgG anti-UCP1 antibody and monoclonal antibody revealed only a few differences in the diameter and density of the particles within the immunoreactive

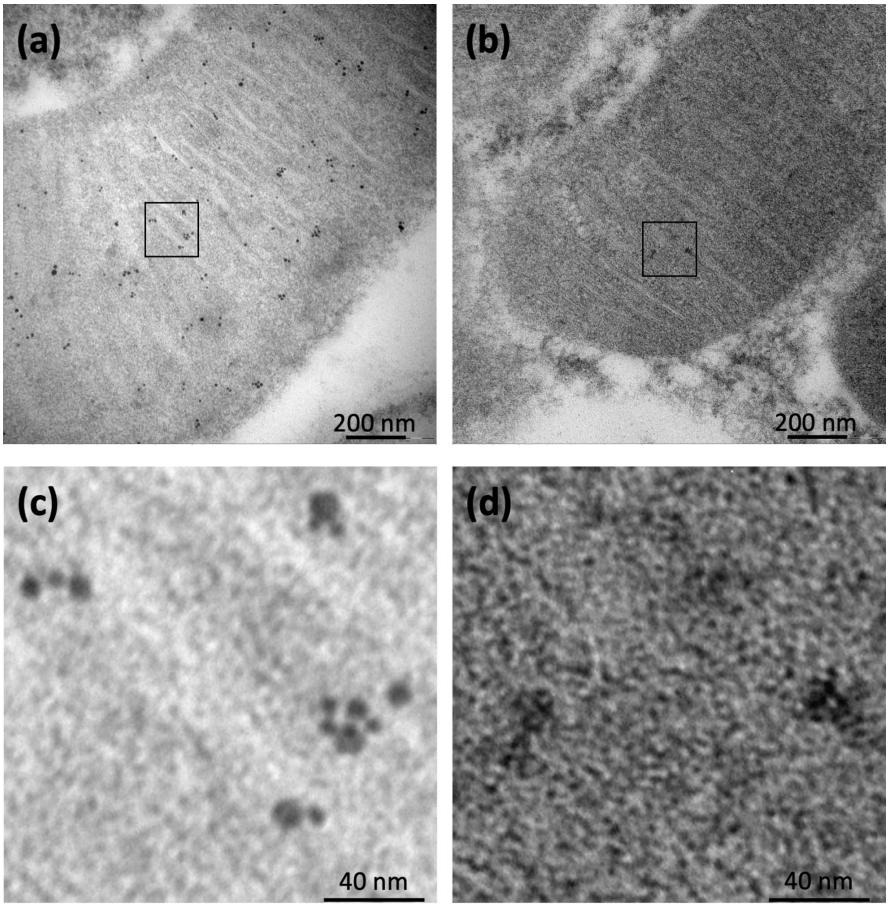

Figure 2. Visualized patterns of gold particles following the monoclonal rabbit IgG treatment of the brown adipose tissue (BAT). Region of interest was focused on the mitochondrial area. (a) UCP1+/G+, scheme A in monoclonal IgG with monoclonal rabbit anti-UCP1 IgG and gold particle-conjugated goat anti-rabbit IgG. Solid aggregation of gold particles was observed in the mitochondrial area. Open square was the domain of the magnification exhibited in c. Solid bar represents 200 nm, ×50,000 magnification. (b) UCP1-/G+, scheme B in monoclonal IgG with polyclonal rabbit IgG and gold particle-conjugated goat anti-rabbit IgG. Faint spots of gold particles were observed in the mitochondrial area. Open square was the domain of the magnification exhibited in below. Solid bar represents 200 nm, ×50,000 magnification. (c) Magnified image of the square in a. The aggregation of massive signals of gold particles was confirmed. Solid bar represents 40 nm, ×200,000 magnification. (d) Magnified image of the square in b. The weak signals of gold particles were observed. Solid bar represents 40 nm, ×200,000 magnification.

clusters (**Figure 3** and **Figure 4**). Statistical evidence underlying the immunoreactive clusters was evaluated by calculating the diameter and density of the immunoreactive particles on the mitochondrial inner crista (**Figure 3** and **Figure 4**). Polyclonal and monoclonal IgG anti-UCP1 antibodies appeared to function similarly as carriers of immunoreactive clusters. The monoclonal IgG anti-UCP1 antibody exhibited clearer immunoreactive clusters, although they were not significantly different from those exhibited by the polyclonal antibody.

The immunoelectron microscopy method was previously established [12]. The immunoreactive clusters of gold particles conjugated to the polyclonal IgG

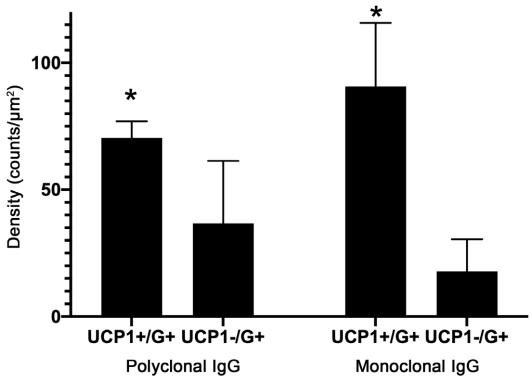

Figure 3. Differences in the densities of the immunoreactive dots of gold particles in the area of mitochondrial inner membranes between groups treated with polyclonal or monoclonal antibody either with or without UCP1 antibody in the brown adipocytes. The vertical and horizontal axes represent the density of immunoreactive dots (counts/μm^2) and the name of the treatment group, respectively. UCP1+/G+, is the group subjected to anti-UCP1 antibody treatment (scheme A). UCP1−/G+, the group without anti-UCP1 antibody treatment (scheme B). G+, the group treated with gold-conjugated goat anti-rabbit IgG antibody. Polyclonal IgG, the group subjected to rabbit polyclonal IgG antibody treatment. Monoclonal IgG, the group subjected to rabbit monoclonal IgG antibody treatment. The density of the group subjected to polyclonal and monoclonal anti-UCP1 antibody combined with gold-conjugated antibody (UCP1+/G+) treatment increased significantly and similarly as compared to that of the group without anti-UCP1 antibody (UCP1−/G+) treatment. Few differences were observed in the density between the polyclonal and monoclonal UCP1+/G+ treatment groups. *P < 0.05.

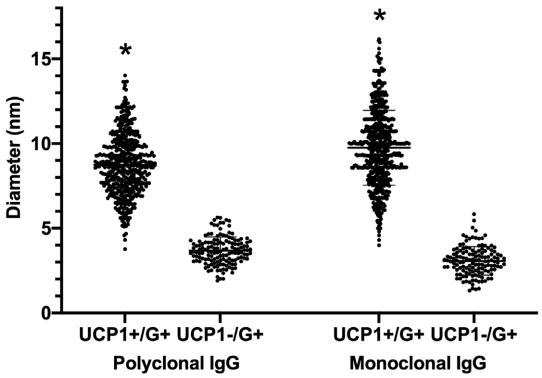

Figure 4. Differences in the diameters of the immunoreactive dots of gold particles in the area of mitochondrial inner membranes between groups treated with polyclonal or monoclonal antibody with or without UCP1 antibody in brown adipocytes. The vertical and horizontal axes represent the diameter of immunoreactive dots (nm) and the name of treatment group, respectively. UCP1+/G+, is the group with anti-UCP1 antibody treatment (scheme A). UCP1−/G+, the group without anti-UCP1 antibody treatment (scheme B). G+, the group subjected to gold-conjugated goat anti-rabbit IgG antibody treatment. Polyclonal IgG, the group treated with rabbit polyclonal IgG antibody. Monoclonal IgG, the group treated with rabbit monoclonal IgG antibody. Next, the diameters of the group subjected to polyclonal and monoclonal anti-UCP1 antibody combined with gold-conjugated antibody (UCP1+/G+) treatment increased significantly and similarly as compared to that of the group without the anti-UCP1 antibody (UCP1−/G+) treatment. Few differences were observed between the polyclonal and monoclonal UCP1+/G+ treatment groups. The line graphs represent the mean and standard deviation. *P < 0.05.

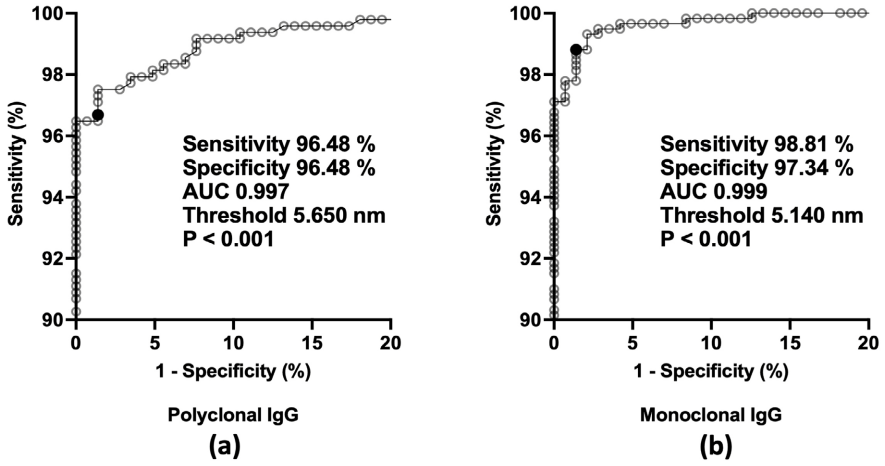

Figure 5. Receiver-operating characteristic curve of the immunoreactive dots of gold particles in the mitochondrial areas of UCP1+/G+ group (scheme A) as compared with that in the UCP1−/G+ group (scheme B). (a) Rabbit polyclonal IgG anti-UCP1 antibody treatment. (b) Rabbit monoclonal IgG anti-UCP1 antibody treatment. The vertical and horizontal axes represent the sensitivity (%) and specificity (%) of the UCP1+/G+ treatment group as compared with those of the UCP1−/G+ treatment group. UCP1+/G+, the group combined with anti-UCP1 antibody and gold-conjugated goat anti-rabbit IgG antibody treatment (scheme A). UCP1−/G+, the group subjected to rabbit IgG and gold-conjugated goat anti-rabbit IgG antibody treatment (scheme B). AUC: area under the curve. High value represents high discrimination capability. Closed circles represent the significant threshold of the diameter. $P < 0.001$ vs UCP1−/G+ group in the univariate binominal logistic regression analysis. The significant true positive values of the diameter of the immunoreactive dots of gold particles were 5.647 nm for the polyclonal UCP1 antibody and 5.140 nm for the monoclonal UCP1 antibody.

anti-UCP1 antibody observed in the mitochondria clearly indicated the site of UCP1 expression in the mitochondria of rats where the protein expression was upregulated upon exposure to cold. Previous studies have quantitatively analyzed immunoreactive clusters of gold particles using immunoelectron microscopy [13] [14] [15] [16] [17]. The accuracy of the diagnostic evaluation using the diameters of immunoreactive gold particles in the logistic regression analysis revealed the significant effective scores for sensitivity and specificity as compared with those of UCP1 antibody and the negative control. The obtained diameter of the immunopositive particles appeared to reflect the manufacturer's data sheet for the diameter of the gold particles. Therefore, we established that verification of the diameters of immunoreactive gold particles could indicate the reliability of the method. Although a few reports have compared the immunohistochemical responses of UCP1 antibody in the BAT between monoclonal and polyclonal IgGs using electron microscopy, our study demonstrated the statistical efficacy of the anti-UCP1 antibody of both polyclonal and monoclonal IgGs using the diameters and densities of the immunoreactive gold particles in the immunoelectron staining of the mouse BAT.

Although our study has a limitation owing to the lack of a stimulus reaction test such as cold exposure or catecholamine beta-3 receptor agonist treatment

where UCP1 might be induced on the inner membrane of the mitochondrial crista of the BAT [1] [2] [3] [20] [21], we demonstrated a significant threshold such as the mean diameter of the gold particle product between immunopositive reactions and nonspecific staining in immunoelectron microscopy. In the future, we intend to clarify the induction of UCP1 expression in the inner membrane of the mitochondrial crista of the BAT in mammals in response to changes in physiological or pathophysiological conditions using immunohistochemical staining and electron microscopy.

Acknowledgements

We thank Shuji Tatsukawa, Aiko Yasuda, and Hiroaki Kawazato for advice on electron microscopy, Yukari Gotoh for advice on light microscopy, and Keisuke Ina and Yoshihisa Fujikura for advice on the organization of this study. We would also like to thank the reviewers of this paper for their detailed feedback.

Conflicts of Interest

The authors declare no conflicts of interest regarding the publication of this paper.

References

[1] Shinde, A.B., Song, A. and Wang, Q.A. (2021) Brown Adipose Tissue Heterogeneity, Energy Metabolism, and Beyond. *Frontiers in Endocrinology* (*Lausanne*), **12**, Article ID: 651763. https://doi.org/10.3389/fendo.2021.651763

[2] Acin-Perez, R., Petcherski, A., Veliova, M., Benador, I.Y., Assali, E.A., Colleluori, G., Cinti, S., Brownstein, A.J., Baghdasarian, S., Livhits, M.J., Yeh, M.W., Krishnan, K.C., Vergnes, L., Winn, N.C., Padilla, J., Liesa, M., Sacks, H.S. and Shirihai, O.S. (2021) Recruitment and Remodeling of Peridroplet Mitochondria in Human Adipose Tissue. *Redox Biology*, **46**, Article ID: 102087. https://doi.org/10.1016/j.redox.2021.102087

[3] Ruan, H.B. (2020) Developmental and Functional Heterogeneity of Thermogenic Adipose Tissue. *Journal of Molecular Cell Biology*, **12**, 775-784. https://doi.org/10.1093/jmcb/mjaa029

[4] Wei, H., Chiba, S., Moriwaki, C., Kitamura, H., Ina, K., Aosa, T., Tomonari, K., Gotoh, K., Masaki, T., Katsuragi, I., Noguchi, H., Kakuma, T., Hamaguchi, K., Shimada, T., Fujikura, Y. and Shibata, H. (2015) A Clinical Approach to Brown Adipose Tissue in the Para-Aortic Area of the Human Thorax. *PLOS ONE*, **10**, e0122594. https://doi.org/10.1371/journal.pone.0122594

[5] Chouchani, E.T., Kazak, L., Jedrychowski, M.P., Lu, G.Z., Erickson, B.K., Szpyt, J., Pierce, K.A., Laznik-Bogoslavski, D., Vetrivelan, R., Clish, C.B., Robinson, A.J., Gygi, S.P. and Spiegelman, B.M. (2016) Mitochondrial ROS Regulate Thermogenic Energy Expenditure and Sulfenylation of UCP1. *Nature*, **532**, 112-116. https://doi.org/10.1038/nature17399

[6] Pinckard, K.M. and Stanford, K.I. (2022) The Heartwarming Effect of Brown Adipose Tissue. *Molecular Pharmacology*, **102**, 460-471. https://doi.org/10.1124/molpharm.121.000328

[7] Hou, D., Fu, H., Zheng, Y., Lu, D., Ma, Y., Yin, Y., Zhang, L. and Bao, D. (2022)

Uncoupling Protein 1 Knockout Aggravates Isoproterenol-Induced Acute Myocardial Ischemia via AMPK/mTOR/PPARalpha Pathways in Rats. *Transgenic Research*, **31**, 107-118. https://doi.org/10.1007/s11248-021-00289-0

[8] Moreno-Santos, I., Macias-Gonzalez, M., Porras-Martin, C., Castellano-Castillo, D., Sanchez-Espin, G., Gomez-Doblas, J.J., de Teresa-Galvan, E. and Jimenez-Navarro, M. (2019) Role of Epicardial Adipose Tissue NPR-C in Acute Coronary Syndrome. *Atherosclerosis*, **286**, 79-87. https://doi.org/10.1016/j.atherosclerosis.2019.05.010

[9] Kortelainen, M.L., Pelletier, G., Ricquier, D. and Bukowiecki, L.J. (1993) Immunohistochemical Detection of Human Brown Adipose Tissue Uncoupling Protein in an Autopsy Series. *Journal of Histochemistry & Cytochemistry*, **41**, 759-764. https://doi.org/10.1177/41.5.8468458

[10] An, Y.A. and Scherer, P.E. (2020) Mouse Adipose Tissue Protein Extraction. *Bio-Protocol*, **10**, e3631. https://doi.org/10.21769/BioProtoc.3631

[11] Diaz Marin, R., Crespo-Garcia, S., Wilson, A.M. and Sapieha, P. (2019) RELi Protocol: Optimization for Protein Extraction from White, Brown and Beige Adipose Tissues. *MethodsX*, **6**, 918-928. https://doi.org/10.1016/j.mex.2019.04.010

[12] Cinti, S., Cancello, R., Zingaretti, M.C., Ceresi, E., De Matteis, R., Giordano, A., Himms-Hagen, J. and Ricquier, D. (2002) CL316,243 and Cold Stress Induce Heterogeneous Expression of UCP1 mRNA and Protein in Rodent Brown Adipocytes. *Journal of Histochemistry & Cytochemistry*, **50**, 21-31. https://doi.org/10.1177/002215540205000103

[13] Cilingir-Kaya, O.T., Moore, C., Meshul, C.K., Gursoy, D., Onat, F. and Sirvanci, S. (2021) Neurogenesis Is Enhanced in Young Rats with Genetic Absence Epilepsy: An Immuno-Electron Microscopic Study. *Turkish Neurosurgery*, **31**, 623-633. https://doi.org/10.5137/1019-5149.JTN.31996-20.2

[14] Alfaro-Ruiz, R., Aguado, C., Martin-Belmonte, A., Moreno-Martinez, A.E. and Lujan, R. (2020) Cellular and Subcellular Localisation of Kv4-Associated KChIP Proteins in the Rat Cerebellum. *International Journal of Molecular Sciences*, **21**, Article 6403. https://doi.org/10.3390/ijms21176403

[15] Martin-Belmonte, A., Aguado, C., Alfaro-Ruiz, R., Albasanz, J. L., Martin, M., Moreno-Martinez, A.E., Fukazawa, Y. and Lujan, R. (2021) The Density of Group I mGlu5 Receptors Is Reduced along the Neuronal Surface of Hippocampal Cells in a Mouse Model of Alzheimer's Disease. *International Journal of Molecular Sciences*, **22**, Article 5867. https://doi.org/10.3390/ijms22115867

[16] Yang, F., Yang, L., Teng, L., Zhang, H. and Katayama, I. (2021) Morphological Alterations and Increased S100B Expression in Epidermal Langerhans Cells Detected in Skin from Patients with Progressive Vitiligo. *Life* (*Basel*), **11**, Article 579. https://doi.org/10.3390/life11060579

[17] Zhou, M., Tanaka, O., Sekiguchi, M., He, H.J., Yasuoka, Y., Itoh, H., Kawahara, K. and Abe, H. (2005) ATP-Sensitive K^+-Channel Subunits on the Mitochondria and Endoplasmic Reticulum of Rat Cardiomyocytes. *Journal of Histochemistry & Cytochemistry*, **53**, 1491-1500. https://doi.org/10.1369/jhc.5A6736.2005

[18] Karnovsky, M.J. (1961) Simple Methods for "Staining with Lead" at High pH in Electron Microscopy. *The Journal of Biophysical and Biochemical Cytology*, **11**, 729-732. https://doi.org/10.1083/jcb.11.3.729

[19] Nagai, K., Noguchi, T., Fujiwara, S., Kawahara, K. and Shimada, T. (2005) Distribution of Langerhans Cells in the Human Esophagus, as Revealed by Immunohistochemistry. *Acta Histochemica et Cytochemica*, **38**, 115-119. https://doi.org/10.1267/ahc.38.115

[20] Reynes, B., Garcia-Ruiz, E., Oliver, P. and Palou, A. (2015) Gene Expression of Peripheral Blood Mononuclear Cells Is Affected by Cold Exposure. *The American Journal of Physiology-Regulatory, Integrative and Comparative Physiology*, **309**, R824-S834. https://doi.org/10.1152/ajpregu.00221.2015

[21] Golic, I., Kalezic, A., Jankovic, A., Jonic, S., Korac, B. and Korac, A. (2020) Insulin Modulates the Bioenergetic and Thermogenic Capacity of Rat Brown Adipocytes *in Vivo* by Modulating Mitochondrial Mosaicism. *International Journal of Molecular Sciences*, **21**, Article 9204. https://doi.org/10.3390/ijms21239204

[22] Nagai, K., Noguchi, T., Fujiwara, S., Kawahara, K. and Shimada, T. (2005) Distribution of Langerhans Cells in the Human Esophagus, as Revealed by Immunohistochemistry. *Acta Histochemica et Cytochemica*, **38**, 115-119. https://doi.org/10.1267/ahc.38.115

[23] Karnovsky, M.J. (1961) Simple Methods for "Staining with Lead" at High pH in Electron Microscopy. *The Journal of Biophysical and Biochemical Cytology*, **11**, 729-732. https://doi.org/10.1083/jcb.11.3.729

[24] Ina, K., Kitamura, H., Tatsukawa, S. and Fujikura, Y. (2011) Significance of Alpha-SMA in Myofibroblasts Emerging in Renal Tubulointerstitial Fibrosis. *Histology & Histopathology*, **26**, 855-866.

Supplementary Data

Material and Methods

Chemicals

For secondary antibodies in the light microscopic analysis, a peroxidase affinipure goat anti-rabbit IgG (111-035-144, Jackson ImmunoResearch Laboratories, West Grove, PA, USA) in combination with an EnVision System (anti-rabbit IgG-HRP conjugated, Dako Inc., Copenhagen, Denmark) and a Texas Red-affinipure goat anti-rabbit IgG (111-075-045, Jackson ImmunoResearch Laboratories, West Grove, PA, USA) in combination with 4',6-diamidino-2-phenylindole dihydrochloride solution (DAPI) (28718-90-3, Dojindo Laboratories, Kumamoto, Japan) were used for immunohistochemical and immunofluorescence staining in the light microscopic observations, respectively. For the development of the physical method (physical development), $AgNO_3$ (Wako Pure Chemical Industries, Ltd., Osaka, Japan), crown ether/dibenzo-18-crown-6 ether (Sigma-Aldrich, St. Louis, MO, USA), and hydroquinone (Wako PureChemical Industries, Ltd., Osaka, Japan) were used. Next, a solution of distilled water 0.1% Kernechtrot (Chroma-Gesellschaft Schmid GmbH & Co, Nordrhein-Westfalen, Germany) and 5% aluminum sulfate (Wako PureChemical Industries, Ltd., Osaka, Japan) were used for nuclear staining in the physical development. Then, hematoxylin (Hx61057849, Merck KGaA, Darmstadt, DE) and eosin (E6003, Sigma-Aldrich, St. Louis, MO, USA) were used for general staining, and 150 mg/kg pentobarbital (Somnopentyl, Kyoritsu Seiyaku Corp., Tokyo, Japan) was applied for deep anesthesia before sample collection.

Apparatus and Software

Fluorescence microscopy (blue in 461 nm, red in 610 nm) examinations were conducted using Eclipse 50i (Nikon Co., Ltd., Tokyo, Japan) and BX60 (Olympus Co., Ltd., Tokyo, Japan), respectively.

Immunohistochemical Staining

Samples that were fixed overnight were dehydrated with ethyl alcohol before embedding in paraffin. Next, coronal serial sections were cut with a thickness of 10 μm and fixed onto MAS-coated glass slides (Matsunami Glass Ind. Ltd., Osaka, Japan). Sections were deparaffinized in xylene, immersed in methanol with H_2O_2 for 30 min at 4˚C, and then hydratedin a series of descending ethanol concentrations before rinsing in running tap water for 5 min. Subsequently, the sections were incubated in 1% BSA in PBS (BSA–PBS; 0.01 M phosphate buffer + 0.15M NaCl, pH 7.2) for 30 min at room temperature (RT) and then incubated with rabbit polyclonal IgG anti-UCP1 primary antibody (1/1000) overnight at 4˚C. Serial sections were rinsed in BSA-PBS for 30 min at RT and incubated in a peroxidase affinipure goat anti-rabbit IgG secondary antibody (1/2000) for 1 h at RT before subjecting them to the EnVision System (for 2 h) and DAB visualiza-

tion (for 10 min) at RT to detect UCP1 immunoreactivity (UCPi). Then, all sections were counterstained with hematoxylin. The specificity of UCP1 antibody was confirmed by performing the same procedure with rabbit polyclonal IgG (1/2000) instead of the primary rabbit polyclonal antibody to UCP1.

Physical Development in Immunogold Silver Staining

The physicalPhysical development is a method for intensifying the immunohistochemical reaction product [1]. The prepared coronal serial sections incubated with the rabbit polyclonal IgG anti-UCP1 primary antibody (1/1000) and rinsed in BSA-PBS similar to immunohistochemical staining were subsequently subjected to immunogold silver staining treatment. The serial sections were incubated in the 6-nm gold-conjugated goat anti-rabbit IgG antibody (1/40) for 1 h at RT, rinsed in 0.01 M PB (pH 7.4) four times for 30 min, and washed with distilled water for 10 s. Next, the physical developer was prepared by mixing distilled water with 10% $AgNO_3$ and 1.1 mM crown ether (solution A) and 0.2 M citric acid buffer (pH 3.45) with 30 mM hydroquinone (solution B). The immediately prepared physical developer was applied to the serial sections for 28 min at 23˚C. After rinsing in running tap water, the serial sections were counterstained with 0.1% Kernechtrot in 5% aqueous aluminum sulfate, rinsed in running tap water, and dehydrated in an ascending ethanol series (more details can be found in our previous report) [22].

Fluorescence Microscopy

The dehydrated sample sections were incubated in 1% BSA in PBS (BSA–PBS; 0.01 M phosphate buffer + 0.15 M NaCl, pH 7.2) for 30 min at RT and then incubated with rabbit polyclonal IgG anti-UCP1 (1/1000) overnight at 4˚C. Then, the serial sections were rinsed in BSA–PBS for 30 min at RT before incubation with Texas Red-affinipure goat anti-rabbit IgG secondary antibody (1/2000) for 1 h at RT in darkness. Then, the sections were rinsed in BSA-PBS for 30 min at RT, after which 1 μg/mL of DAPI was applied.

Transmission Electron Microscopy

The collected samples were cut into very fine pieces, fixed in 50% Karnovsky's fixative [23] for 10 min at 4˚C, rinsed with 0.1 M cacodylate buffer (pH 7.4), and post-fixed in 2% OsO_4 (0.1 M cacodylate buffer with 1% potassium ferrocyanide) for 2 h at 4˚C. The specimens were dehydrated in an ascending ethanol wash series and embedded in epoxy resin. Ultrathin sections were cut using an ultramicrotome, mounted on copper grids, and stained with methanolic uranyl acetate and lead citrate. Ultrathin sections were evaluated by Transmission electron microscopy (TEM) at an accelerating voltage of 80 kV [24].

Supplementary Results

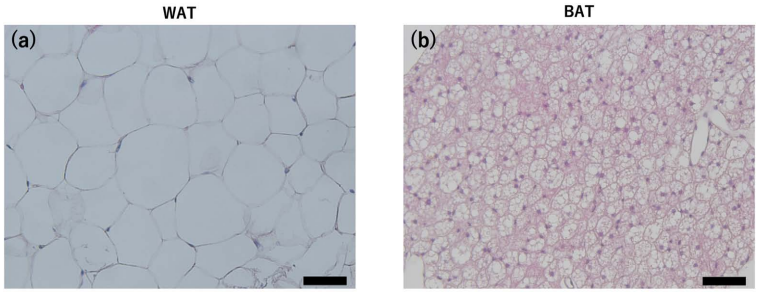

Figure S1. Histological overview of white adipose tissue (WAT) and brown adipose tissue (BAT) in hematoxylin-eosin staining. (a) WAT with thin cytoplasm and vast cavities with fat droplets. (b) BAT expressed a multilocular aspect distinguished by relatively thick cytoplasm and small cavities, representing smaller fat droplets. Solid bar represents 50 μm.

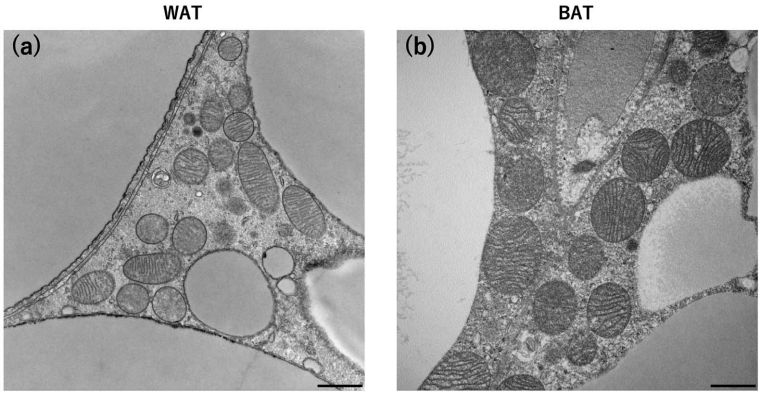

Figure S2. Ultra-structural Ultrastructural aspect of white adipose tissue (WAT) and brown adipose tissue (BAT) examined by transmission electron microscopy. (a) White adipocyte (WAC) with thin cytoplasm and vast cavities with fat droplets. The mitochondria in the cytoplasm were small and scarce. (b) Brown adipocyte (BAC) exhibited well-developed mitochondria and relatively abundant cytoplasm compared to that of WAC. Solid bar represents 1 μm.

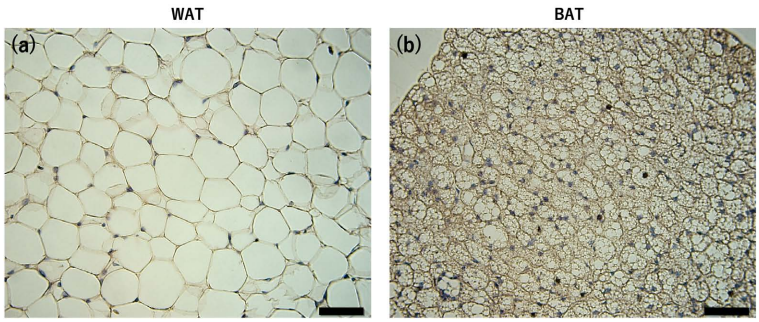

Figure S3. Immunohistochemical staining of WAT and BAT using EnVision. (a) White adipose tissue (WAT) showed few signals of immunoreactive staining in the cytoplasm. (b) Brown adipose tissue (BAT) showed significant signals in brown, suggesting the expression of UCP1 in the cytoplasm. Solid bar represents 50 μm.

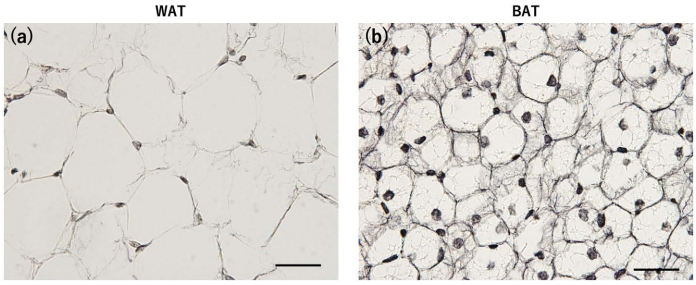

Figure S4. Immunohistochemical staining of WAT and BAT using the physical development method. (a) White adipose tissue (WAT) showed few signals of immunoreactive staining in the cytoplasm. (b) Brown adipose tissue (BAT) showed significant signals in black, suggesting the expression of UCP1 in the cytoplasm. Solid bar represents 40 μm.

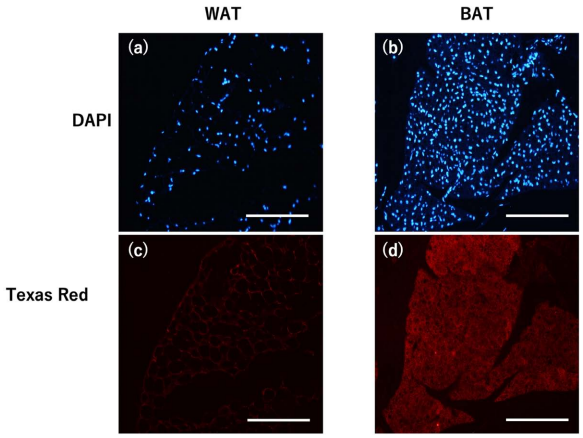

Figure S5. Immunohistochemical staining of WAT and BAT with the fluorescence method using Texas Red and DAPI. (a) White adipose tissue (WAT) showed high signals of DAPI staining representing the nucleus. (b) Brown adipose tissue (BAT) showed significant signals of DAPI staining in the cytoplasm. (c) Whereas few signals were found in the cytoplasm. (d) Accompanied with signals of Texas Red, implying the expression of UCP1. Solid bar represents 200 μm.

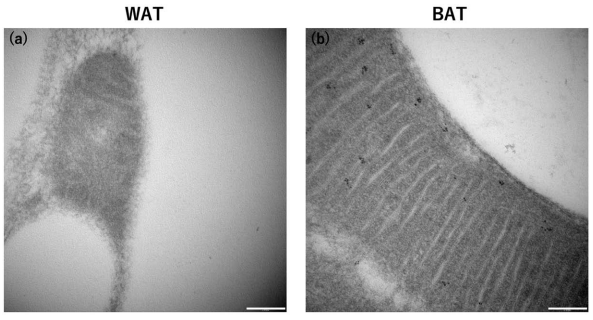

Figure S6. Immunoelectron staining with rabbit polyclonal IgG anti-UCP1 antibody combined with gold-conjugated anti-rabbit IgG antibody compared between white adipose tissue (WAT) and brown adipose tissue (BAT). (a), White adipocyte (WAC) showed no signals of gold particles of 5.4 nm in the cytoplasm, especially in the area of mitochondrial inner membrane. (b), Brown adipocyte (BAC) showed high-intense signals of gold particles of 5.4 nm in the area of mitochondrial inner membrane. The intense signals highly indicated the presence of UCP1 at the mitochondrial inner membrane of the brown adipocytes of mouse. Solid bar represents 200 nm.